

RSC Advances



This is an *Accepted Manuscript*, which has been through the Royal Society of Chemistry peer review process and has been accepted for publication.

Accepted Manuscripts are published online shortly after acceptance, before technical editing, formatting and proof reading. Using this free service, authors can make their results available to the community, in citable form, before we publish the edited article. This *Accepted Manuscript* will be replaced by the edited, formatted and paginated article as soon as this is available.

You can find more information about *Accepted Manuscripts* in the [Information for Authors](#).

Please note that technical editing may introduce minor changes to the text and/or graphics, which may alter content. The journal's standard [Terms & Conditions](#) and the [Ethical guidelines](#) still apply. In no event shall the Royal Society of Chemistry be held responsible for any errors or omissions in this *Accepted Manuscript* or any consequences arising from the use of any information it contains.

Cite this: DOI: 10.1039/c0xx00000x

www.rsc.org/xxxxxx

ARTICLE TYPE

Facile solvothermal synthesis of 3D flowerlike β - In_2S_3 microspheres and their photocatalytic activity performance

Caiying Wei,^{a,b} Wei Guo,^{a,b} Jiaqin Yang,^{a,b} Hongmin Fan,^{a,b} Jing Zhang^{a,b} and Wenjun Zheng^{*a,b}

Received (in XXX, XXX) Xth XXXXXXXXX 20XX, Accepted Xth XXXXXXXXX 20XX

DOI: 10.1039/b000000x

Three-dimension (3D) flowerlike β - In_2S_3 microspheres have been successfully synthesized by a facile solvothermal method using thioacetamide (TAA, CH_3CSNH_2) as both sulfur source and ligand of In^{3+} in ethanol-water system. The morphologies of In_2S_3 can be controlled by simply changing the volume ratio of ethanol to water in solvent. The experimental results demonstrate that 3D flowerlike β - In_2S_3 microspheres undergo surface recrystallization, selective absorption and oriented growth processes. A detailed morphology formation mechanism has been proposed and discussed. Furthermore, the 3D flowerlike β - In_2S_3 microspheres show relatively high visible-light photocatalytic activity for methyl orange (MO) degradation, which can be attributed to both the relative higher BET surface area and advantageous optical property.

15 Introduction

In quest of environmental purification, photocatalysis using semiconductors and light energy has attracted tremendous attention. The most extensively studied photocatalyst, TiO_2 ^[1], possesses a wide band gap 3.0-3.2 eV, which is only active under irradiation of ultraviolet (UV) light accounting for ~4% of the total sunlight^[2]. To effectively harvest the visible light that is the most abundant in the total sunlight, much work has been done to develop the “second-generation” TiO_2 by dye sensitizing and doping^[3-8], which unfortunately can either not show an ideal absorption in the visible-light region or be unstable during the photocatalysis process. In recent years, more and more attention has been paid to developing new visible-light-active photocatalysts (e.g., Ag_3PO_4 ^[9], Ag_3VO_4 ^[10], BiVO_4 ^[11], CdS/graphene ^[12], ZnInS_2 ^[13]). However, these photocatalysts are unstable upon illumination with light (e.g., Ag_3PO_4 , Ag_3VO_4), exhibit low activity (e.g., BiVO_4), include highly toxic element (e.g., CdS) or difficult to control synthesis (e.g., ZnInS_2). Compared with above mentioned photocatalysts, the cost of Indium sulfide (In_2S_3) is relatively high, because indium is a kind of dispersed element. However, In_2S_3 has tremendous advantages, due to its excellent illumination stability^[14], superior visible light activity^[15-17], stable chemical and physical characteristics and low toxicity^[17, 18]. At atmospheric pressure, In_2S_3 is found to crystallize into three different structural forms, defective cubic structure (α - In_2S_3), defective spinel structure (β - In_2S_3), and layered hexagonal structure (γ - In_2S_3)^[19-30]. β - In_2S_3 is the stable state at room temperature with a tetragonal structure or cubic form, which is an n-type semiconductor with a suitable band gap of 1.9-2.3 eV corresponding to visible light region^[31].

It is well-known that the size and morphology of nanomaterials have an important influence on their properties, such as the

movement of electrons and holes and the transportation related to phonons^[32, 33]. Especially micrometer 3D architecture with nano-scale building blocks is effective during the photocatalysis application, considering the enhanced light-harvesting capacity^[34], the prevention of aggregation and the easy solid/liquid separation. Morphologically distinct 3D nanocrystals of In_2S_3 including 3D chrysanthemum-like superstructures^[35, 36], half shells^[37], micropompons^[38], hollow microspheres^[16, 39], porous 3D flowerlike structures^[21, 40] have been prepared by various methods. However, among these methods some depend on poisonous organic solvents as the reaction mediates, some demand the surfactants as templates and some need complex or highly toxic sulfur source to control ions activity. Therefore, how to obtain the desired 3D micrometer architectures of In_2S_3 using simple method is still in need of further exploration.

Herein, we put forward a facile solvothermal strategy to synthesize 3D flowerlike β - In_2S_3 hierarchical superstructure assembled by two-dimension (2D) In_2S_3 nanosheet building blocks. In this method, TAA acts both as sulfur source and ligand of In^{3+} , which plays an important role in the phase and shape formation of In_2S_3 . Compared with the aforementioned methods, simplicity and safety make our pathway dominant (using TAA as sulfur supplier which is a common and harmfullness sulfur source, applying nontoxic ethanol-water mixed solvent as reaction system and without any surfactants). Moreover, morphologies of the In_2S_3 can be controlled by simply changing the volume ratio of water and ethanol. The possible growth mechanism of 3D flowerlike In_2S_3 microspheres is proposed and discussed. Further physical investigations reveal that the unique hierarchical superstructure greatly depends upon the synthesis condition. In addition, the prepared 3D flowerlike In_2S_3 microspheres are applied in photocatalytic degradation of MO to investigate its photocatalytic properties, which show relatively high visible-light

photocatalytic activity.

Experimental procedure

Synthesis of 3D flowerlike In_2S_3 microspheres

In a typical procedure, $\text{InCl}_3 \cdot 4\text{H}_2\text{O}$ (0.5 mmol) and TAA (3 mmol) were dissolved in a mixed solvent of distilled water (10 mL) and absolute ethanol (10 mL) under constant vigorous stirring to yield a homogeneous solution. Then, the solution was transferred into a 33 mL capacity Teflon-lined stainless steel autoclave. The autoclave was sealed and maintained at 180 °C for 24 h, and then allowed to cool to room temperature. The resulting powders were filtered and washed with distilled water and absolute ethanol several times to remove the by-products, and finally dried at 60 °C for 4 h under vacuum.

Characterization

The phase compositions of the products were characterized by X-ray diffraction (XRD) on a Rigaku D/max 2500V/PC X-ray diffractometer with Cu-K α radiation ($\lambda = 1.54056 \text{ \AA}$). The morphologies of the products were examined with a JSM 6700F scanning electron microscope (SEM). The element analysis was conducted with an energy-dispersive spectrometer (EDS), an accessory of SEM (JSM 6700F). The transmission electron microscopy (TEM) and high-resolution TEM (HRTEM) micrographs were taken with a Tecnai G2 F20 transmission electron microscope. The Brunauer-Emmett-Teller (BET) specific surface area was measured by using the nitrogen adsorption-desorption isotherms (BELSORP-Mini) at 77 K. A Shimadzu UV-3600 UV-vis spectrophotometer was used to record the UV-vis diffuse reflection spectroscopy (DRS) of the samples. The photoluminescence (PL) spectra of the products were obtained by a fluorescence lifetime and steady state spectrometer (FSP 920) with an excitation wavelength of 322 nm.

Photocatalytic Reactions

The photocatalytic activities of the obtained In_2S_3 products were evaluated by the photocatalytic degradation of MO aqueous solution at room temperature under visible light irradiation. A 250 W Xe lamp with a cutoff filter for UV light and a water cutoff filter for infrared light were used as a light source to provide the visible light. In the test, 0.05 g of as-prepared In_2S_3 dispersed into 100 mL of MO aqueous solution (10 ppm). Before light irradiating, the suspension stirred for 30 min in the dark to reach an adsorption-desorption equilibrium between the photocatalyst and MO solution. At given time intervals, 5 mL aliquots were extracted and centrifuged to remove the In_2S_3 nanocrystals. The filtrates were analyzed by recording variations of the maximum absorption band ($\lambda = 464 \text{ nm}$) in the UV-vis spectra of MO using UV-vis spectrophotometer.

Results and discussion

The phase composition of the In_2S_3 nanocrystals obtained in ethanol-water system with the volume ratio of 1:1 for 24 h is investigated by XRD. As shown in Figure 1a, all these peaks are indexed to the diffraction pattern of cubic $\beta\text{-In}_2\text{S}_3$, meanwhile, the structural parameter of $a = 10.774 \text{ \AA}$ agrees very well with the reported values (JCPDS Card No. 65-0459). Comparing with the

standard XRD pattern, the intensity of the (222) peak is strengthened, and, in order to clearly observe the changes of (222), the fitting curve of XRD pattern from 26° to 29.5° is presented in Figure S1. The intensity ratio of $I_{(222)}/I_{(311)}$ increases from 0.099 to 0.540 corresponding to standard value and experimental value, respectively, implying the (222) facets have been preferentially exposed.

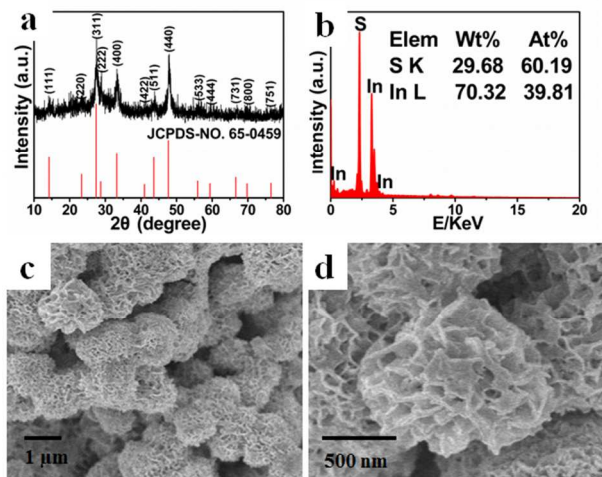


Figure 1 (a) XRD, (b) EDS, (c) SEM and (d) high-magnification SEM of 3D flowerlike In_2S_3 microspheres obtained in ethanol-water system with the volume ratio of 1:1 for 24 h.

No characteristic peak is observed for other impurities such as InS, In, and S, indicating that pure cubic $\beta\text{-In}_2\text{S}_3$ is formed via the solvothermal process. An EDX spectrum (Figure 1b) of the products is recorded to analyze chemical compositions of In_2S_3 nanocrystals. The result suggests that uniform 3D flowerlike In_2S_3 microspheres only consist of indium and sulfur with an atomic ratio of 60.19:39.81, which is almost consistent with the stoichiometry of In_2S_3 . The morphologies of In_2S_3 nanocrystals are studied by SEM. As shown in the low-magnification SEM image (Figure 1c), the obtained product is composed by many uniform 3D flowerlike microspheres with diameter about 1 μm presenting with imperfect dispersibility. It can be clearly revealed in high-magnification SEM image (Figure 1d) that the exterior surface of In_2S_3 microsphere exhibits an extensive growth of sheet-like structures. The thickness of these nanosheets mostly is about 10 nm, and these nanosheets align together at different orientation, forming open cavities distributed on the entire surface of the microspheres. The cavities are a few tens of nanometers in width and a few tens of nanometers in deep with the pinnacles pointing to the center of the microspheres. It is expected that such cavities may lead to cavity-mirror effects and large specific surface area.

TEM characterization may provide additional information regarding the interior structure of these architectures. A typical TEM image is shown in Figure 2a, the dark center of the microsphere suggests that the microsphere has a solid central part while the pale area along the perimeter indicates that the perimeter of the microsphere is built by very thin sheets, which is consistent with the SEM images. A HRTEM image taken at the fringe of In_2S_3 nanosheet is displayed in Figure 2b, which presents crystalline structural information on the In_2S_3 nanosheet.

These nanosheets show a highly single-crystalline, determined by the large-scale clear and regular lattice fringes.

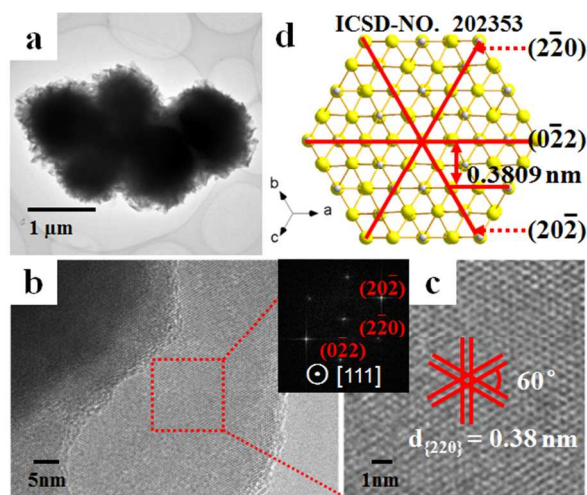


Figure 2 (a) TEM, (b) HRTEM, (c) enlarged HRTEM images, (inset) corresponding FFT pattern of 3D flowerlike In_2S_3 microspheres obtained in ethanol-water system with the volume ratio of 1:1 for 24 h, and (d) crystal structure of cubic In_2S_3 viewed along the [111] direction (● S and ○ In).

For better visibility of the lattice fringes, enlarged HRTEM image taken from the square areas has been shown in Figure 2c. The typical lattice fringe spacing is certified to be 0.38 nm, corresponding to the {220} crystallographic plane families of cubic $\beta\text{-In}_2\text{S}_3$, indicating the preferential growth along the $\langle 220 \rangle$ crystallographic direction families. The corresponding hexagonal symmetrical fast Fourier transform (FFT) pattern (inset) further demonstrates that the obtained In_2S_3 nanosheet is in single crystalline structure with preferential growth along the $\langle 220 \rangle$ crystallographic direction families. Moreover, the quasi-hexagonal-shaped FFT pattern is a typical feature of the reciprocal lattice projected along the [111] zone axis of cubic $\beta\text{-In}_2\text{S}_3$ [15, 27, 41], which confirms that the exposed facet is (222) plane, consistent with the XRD result. A typical atomic model obtained from ICSD-202353 is shown in Figure 2d, further revealing its hexagonal symmetrical structure viewed along the [111] direction.

In order to disclose the formation mechanism of 3D flowerlike In_2S_3 microspheres, the whole synthesis process has been carefully observed and analyzed, including the dissolution process of reactants at room temperature and the reaction process in the high temperature oven. At first, when $\text{InCl}_3 \cdot 4\text{H}_2\text{O}$ and excess TAA are added to the mixed solvent of ethanol (10 mL) and water (10 mL), uniform and transparent solution can be obtained immediately. Then, the solution is transferred into Teflon-lined stainless steel autoclave and kept for several hours in oven. The products obtained at different reaction durations in the autoclave is collected and analyzed through XRD (Figure S2) and SEM (Figure 3). It could be found that all of the XRD peaks can be readily indexed to cubic $\beta\text{-In}_2\text{S}_3$ phase (JCPDS No. 65-0459) and the intensity of the diffraction peaks has hardly changed, however, the intensity of the (222) peak begins to increase from 2 h and gradually enhances with the reaction time prolonging. This observation implies that the crystal growth of

In_2S_3 gets down to adopting oriented growth along $\langle 220 \rangle$ crystallographic direction families to expose (222) facet from 2 h. The corresponding SEM images further evidence the shape evolution process of 3D flowerlike In_2S_3 microspheres.

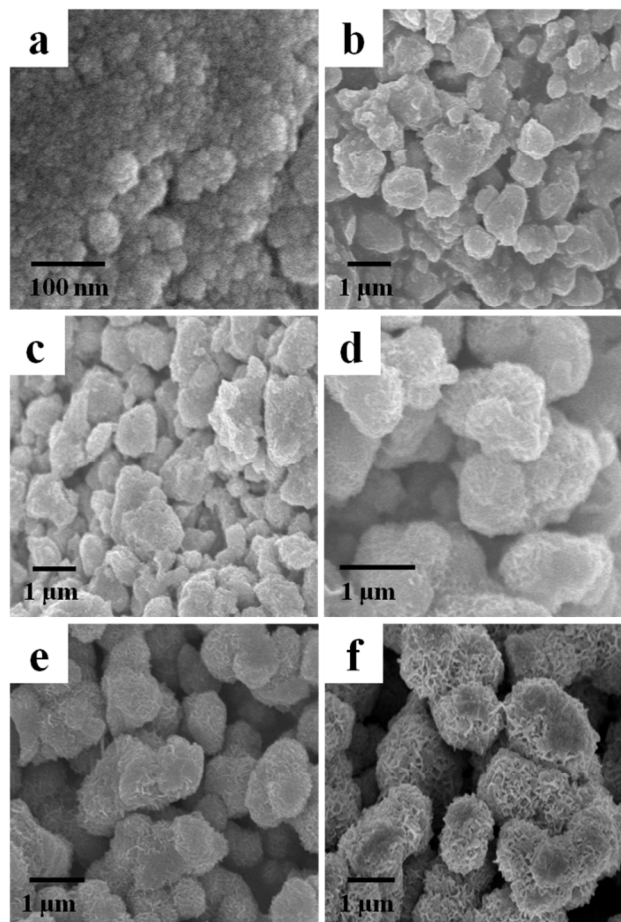


Figure 3 SEM images of In_2S_3 nanocrystals synthesized at different reaction durations in ethanol-water system with the volume ratio of 1:1: (a) 0.5 h, (b) 1 h, (c) 2 h, (d) 4 h, (e) 8 h, (f) 16 h.

From Figure 3a to Figure 3f, we could find that small In_2S_3 nanoparticles about 10 nm in diameter are the exclusive products for 0.5 h (Figure 3a), and then large microspheres with several hundred nanometers in diameter gradually appear when the reaction time is prolonged to 2 h (Figure 3b and 3c). After 2 h (Figure 3d), a great number of small nanosheets begin to grow on the surface of the microspheres resulting in the preferential exposure of (222) facet. As time going on (Figure 3e and 3f), the nanosheets continually grow up and the diameters of these microspheres develop from several hundred nanometers to about 1 μm .

On the basis of the dissolution process of reactants and the above experimental results, we deduce the formation mechanism of 3D flowerlike In_2S_3 microspheres, pictorially shown in Figure 4. The fast dissolution process of reactants indicates the excess TAA can coordinate with In^{3+} completely and form indium-TAA complexes rapidly, which greatly promote the dissolution of $\text{InCl}_3 \cdot 4\text{H}_2\text{O}$ and avoid hydrolysis and precipitation of In^{3+} [13, 42, 43]. This ensures a homogeneous environment during the reaction procedure, and makes the reaction carry out in a very low rate to

obtain nanocrystals with perfect crystal structure and morphology. Indeed, In^{3+} can form two different complexes with TAA as the tetrahedral $[\text{In}(\text{TAA})_4]^{3+}$ and the octahedral $[\text{In}(\text{TAA})_6]^{3+}$ [13, 43]. During the reaction process, along with the rise of temperature and pressure, S^{2-} ions are slowly released by TAA when the violent shaking S-C bond of TAA is broken under the powerfully nucleophilic attack of high-energy water molecules, and as a result, In-S_6 and In-S_4 species are formed [13, 16, 43]. Then, these freshly generated metal sulfur species combine in situ to reduce their charge density, resulting in a thermodynamically stable cubic phase In_2S_3 nuclei in which the coordination pattern of the ions in solid retain the same style as in the solution. In other words, the coordination manner of the ions in the solution can determine the phase of the solid product [43].

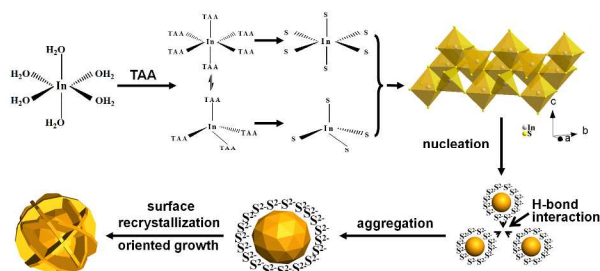


Figure 4 The proposed growth mechanism of 3D flowerlike In_2S_3 microspheres.

At this initial stage, a large number of In_2S_3 nuclei can form in a short time due to the excess S^{2-} , resulting in a high degree supersaturation of In_2S_3 . Large amounts of small In_2S_3 nanoparticles are further obtained with the continuous supply of the building blocks. At the same time, surplus S^{2-} tends to attach to the surface of products for the electrostatic interaction between S^{2-} and In^{3+} on the surface. These particles in the solution can aggregate to form large microspheres, driven by minimizing the surface energy and hydrogen-bond interaction [16, 44, 45]. There are large amounts of hydrogen bonds in ethanol-water system which can supply enough interaction force to involve in the process. The plentiful sulfur ions surrounding the microspheres can recombine with solid In_2S_3 to generate liquid In-S_6 or In-S_4 species. Therefore, as time going on, the In_2S_3 on the surface of microsphere dissolve and recrystallize to form sheetlike In_2S_3 nuclei which is bounded by alternant $\{110\}$ and $\{222\}$ facets [15]. This dissolution and recrystallization process on the microsphere surface is decisive for the formation of sheetlike structure. It is worth noting that In_2S_3 molecules generated rate at this stage slows down due to the low concentration of reactants. As a consequence, the concentration of In_2S_3 molecules is not enough for the former microspheres to grow from the circumference. The new generated building molecule blocks will preferentially occur at the sheetlike In_2S_3 nuclei which are active sites with higher free energies [46]. Generally, the final crystal shape is the cooperative result of internal crystal factors and external reaction factors [47]. According to Gibbs-Wulff's theorem, higher surface tension faces tend to grow along its normal direction and eventually disappear from the final appearance, and a sequence of $\gamma_{\{222\}} < \gamma_{\{110\}}$ can be easily obtained for the cubic phase in light of this theorem [15]. Moreover, in our experiment, TAA might further cap on the (222) plane of In_2S_3 and increase the difference

of surface energy between (222) and (110) planes. As shown in Figure S3, the (222) plane of cubic In_2S_3 is completely composed by In^{3+} , which is facile for the TAA to adsorb to the surface of (222) plane and coordinate with In^{3+} . Consequently, the growth of the In_2S_3 crystal along [111] direction is suppressed and In_2S_3 crystal growth mainly processes along the six symmetric directions to form sheetlike In_2S_3 . Finally, a flowerlike structure is formed by selective absorption and oriented growth on active sites [48]. Besides, it may be due to the presence of large amounts of hydrogen bond in ethanol-water system that the 3D flowerlike In_2S_3 microspheres aggregate in a certain degree during the formation process. Based on the above results, the possible overall chemical reactions that occurred during the formation of In_2S_3 could be proposed as shown in Equ. (1)-(3) [49]:

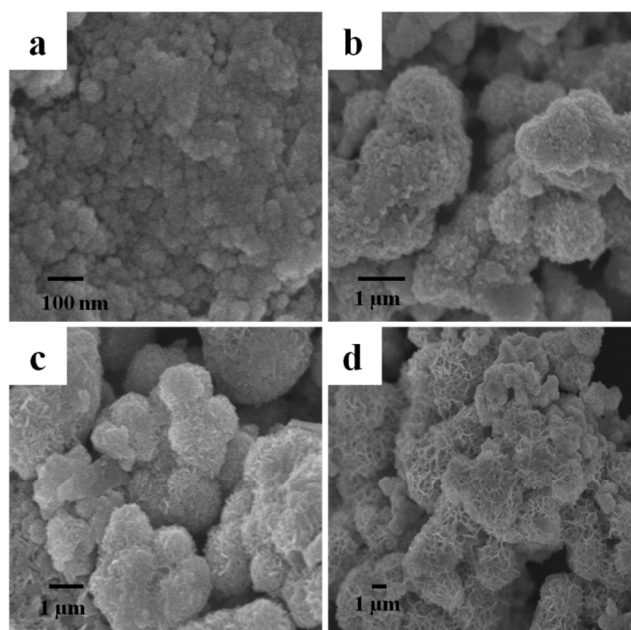
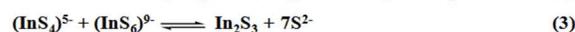
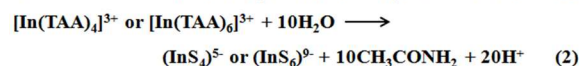
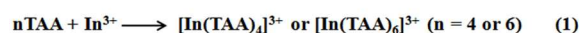


Figure 5 SEM images of products obtained in ethanol-water system with the volume ratio of: (a) 1:0, (b) 3:1, (c) 1:3, (d) 0:1.

In general, the reaction environment has a great effect on the morphology of the final products. Our experimental results indicate that the solvents indeed play an important role in the formation of products. As can be observed in Figure S4, all of the XRD peaks can be readily indexed to cubic $\beta\text{-In}_2\text{S}_3$ phase (JCPDS No. 65-0459), however, the intensity of the (222) peak gradually increases with the water dosage improving. It indicates that increasing the water dosage is conducive for the formation of sheetlike structure. SEM images in Figure 5 further verify the effect of water on the formation of nanosheets. Nanoparticles and out-of-shape microcrystals composed by nanoparticles with compact structure (Figure 5a, 5b) are obtained in pure ethanol or ethanol-water system with the volume ratio of 3:1, respectively. Adjusting the volume ratio of ethanol and water into 1:3, aggregate structures of flowerlike microspheres are obtained. On

the surface of these structures, large amounts of interlinked nanosheets form plenty of open cavities (Figure 5c). In pure water, numerous microcrystals composed by interlaced In_2S_3 nanosheets aggregate and weld together, in which numerous well-developed open cavities are also observed (Figure 5d). Based on the decomposition equation of TAA, increasing the amount of water molecules can promote the decomposition reaction and generate more S^{2-} . Thus, in this system with more water, there will be more S^{2-} surrounding the products, which greatly facilitate the In_2S_3 dissolution and recrystallization to form sheetlike nuclei on the surface of products and is conducive for the formation of sheetlike structure. Moreover, it is obvious that aggregation of nanocrystals is also attributed to the adding of the water. It could be owing to the more abundant hydrogen bond network in the solvent [50]. According to the above discussion and experimental results, morphologies of the In_2S_3 can be controlled by simply changing the volume ratio of water and ethanol in solvent. The best volume ratio of ethanol and water to synthesize desired product is 1:1, which can make the products possess both sheetlike loose structure and better dispersibility.

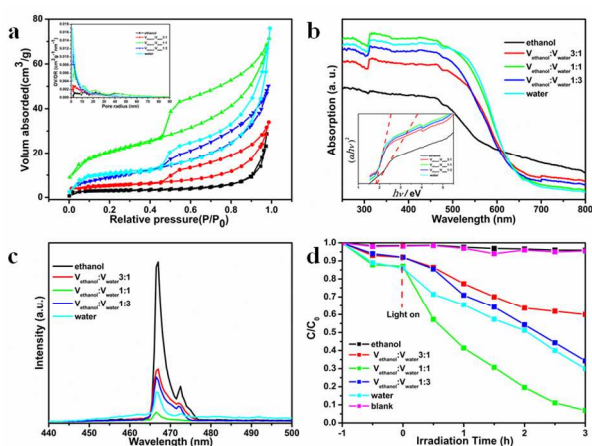


Figure 6 (a) Nitrogen adsorption-desorption isotherm (inset: BJH pore size distribution plot); (b) UV-vis DRS spectra (inset: plots of $(\alpha h\nu)^{1/2}$ vs $h\nu$); (c) room temperature PL spectra of as-synthesized products in 25 different solvents and (d) photocatalytic degradation curve of MO (10 ppm) degradation applying In_2S_3 obtained in different solvents (blank: with visible light irradiation but without any photocatalysts).

The specific surface area is an important property of a catalyst to determine its activity to apply for photocatalytic degradation. Large surface areas can effectively reduce the e^-/h^+ recombination rate, which will lead to more efficient reaction with the oxidant to produce radicals for dye degradation or directly reaction with the dyes [51, 52]. The BET specific surface areas of obtained samples in different solvents are calculated from the nitrogen adsorption-desorption isotherms. As can be seen from Figure 6a, the isotherms are characteristic of type IV isotherms with a hysteresis loop. 3D flowerlike In_2S_3 powder possesses the largest BET surface area of $72.9 \text{ m}^2 \text{ g}^{-1}$, which may be attributed to its loose flowerlike structure and better dispersibility. As speculated, In_2S_3 samples with other compact or aggregate shapes have smaller specific surface areas. The specific surface areas of nanoparticles and microcrystals composed by nanoparticles with compact structure are just $10.4 \text{ m}^2 \text{ g}^{-1}$ and $18.3 \text{ m}^2 \text{ g}^{-1}$, which are obtained in pure ethanol or ethanol-water system (3:1), respectively.

Aggregate structures of flowerlike microspheres synthesized in ethanol-water system (1:3) and pure water possess surface area of $33.7 \text{ m}^2 \text{ g}^{-1}$ and $38.1 \text{ m}^2 \text{ g}^{-1}$, respectively. In addition to the structural properties, the optical properties of the In_2S_3 samples are also studied by UV-vis DRS and PL spectra. Figure 6b shows the typical UV-vis diffuse reflectance spectra of the as-synthesized In_2S_3 nanocrystals. The wide and intense absorption peaks in ultraviolet and visible region reveal strong absorption of ultraviolet light and visible light. Comparing with other products, In_2S_3 composed by nanosheets with more cavities show stronger absorption which are obtained in ethanol-water system (1:1, 1:3) and pure water. Because, open cavities are conducive to their excellent cavity-mirror effect, leading to a great improvement of the reflection and absorption ability for laser [53]. Photons inside the cavities have little chance to escape as they will be reflected many times until most of them are finally absorbed. The calculated pore volume using Barrett-Joyner-Halenda (BJH) method (Table 1) further indicates that the products composed by nanosheets possess more pores. According to the pore size distribution plots (inset of Figure 6a) of samples, the pore size is not uniform ranging from a few nanometers to a few tens nanometers, which is consistent with the TEM observation. For an indirect gap semiconductor, it is well-known that the relation between absorption coefficient and band gap energy can be described by the formula $(\alpha h\nu)^{1/2} = A(h\nu - E_g)$ (where α , $h\nu$, and E_g are the absorption coefficient, the discrete photon energy, and the band gap energy, respectively; A is a constant) [14]. A classical extrapolation approach is employed to estimate the E_g of In_2S_3 products. The extrapolated value (the straight line to the X axis) of $h\nu$ at $\alpha = 0$ give the band gap E_g of approximate 1.9 eV (inset of Figure 6b) which agrees with the experimental reports [54]. These samples have almost no difference in the band gap energy. It may be due to the size of their building blocks is similar and is not enough to cause quantum confinement effect [55]. The specific surface area, pore volume, pore size distribution and E_g of different samples are summarized in Table 1.

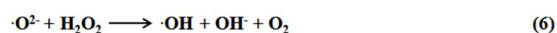
Table 1 Measured parameters for the samples synthesized in different solvents.

Sample	Surface area ($\text{m}^2 \text{ g}^{-1}$)	Pore volume ($\text{cm}^3 \text{ g}^{-1}$)	Average pore size (nm)	E_g (eV)
ethanol	10.412	0.0489	18.783	1.91
$V_{\text{ethanol}}:V_{\text{water}}$ 3:1	18.324	0.0526	11.472	1.90
$V_{\text{ethanol}}:V_{\text{water}}$ 1:1	72.928	0.1149	12.076	1.93
$V_{\text{ethanol}}:V_{\text{water}}$ 1:3	33.692	0.0774	9.1960	1.89
water	38.074	0.1104	6.0572	1.92

PL spectra originate from the migration, transfer, and separation efficiency of the photogenerated charge carriers in a semiconducting material. There is a strong correlation between PL intensity and the photocatalytic performance. Higher PL intensity indicates the higher recombination of the charge carriers, which results in lower photocatalytic activity. The comparison of PL spectra of the as-synthesized In_2S_3 nanocrystals for excitation wavelength 322 nm is shown in Figure 6c. The two emission peak centers at 467 nm and 472 nm can be attributed to the presence of several deep trap states or defects in the structure [25, 37, 40]. As we mentioned above, large specific surface area indeed effectively reduce the recombination rate of the charge carriers. Comparing Figure 6c with Figure 6a, it can be discovered that the order of PL intensity is on contrary to the specific surface area of

products. And 3D flowerlike In_2S_3 products which have the largest specific area possess the minimum relative intensity of PL spectra. Consequently, the advantageous optical property and large specific surface area may endow the as-prepared 3D flowerlike In_2S_3 microspheres with the best potential applications of effective photocatalysis under visible-irradiation in our experiment.

The visible-light photocatalytic activity of 3D flowerlike In_2S_3 microspheres, and some comparative experiments were evaluated by degradation of MO aqueous solution. Under visible-light irradiation, the photocatalytic results of MO are showed in Figure S5 and 6d. Temporal changes in the concentration of MO as monitored by the maximal absorption in UV-vis spectra at 464 nm over the 3D flowerlike In_2S_3 microspheres are showed in Figure S5. It is found that the intensity of the absorption peak of MO is decreased gradually with the irradiation time increasing, accompanied with the color change from the initial orange to nearly colorless. Meanwhile, the main absorption peak position has almost no change and no other absorption band appears, which suggests that the whole process is dominated by photocatalytic degradation mode other than dye sensitization. Figure 6d shows the variation in absorption of MO at 464 nm with the passage of irradiation time. The y-axis of degradation is reported as C/C_0 , C is the absorption of MO at each irradiated time interval of main peak of absorption spectrum at wavelength 464 nm and C_0 is the absorption of starting concentration. As shown in Figure 6d, left of dotted line, the absorption-desorption equilibriums are established after 30 min in dark absorption of In_2S_3 photocatalysts, so the light was turned on after 60 min of dark absorption. The blank experiment without In_2S_3 photocatalyst indicates that direct photocatalysis of MO under the same conditions can almost be neglected. After visible light irradiation 30 min, MO is degraded by 42.7% over as-prepared 3D flowerlike In_2S_3 microspheres and 93.1% for 180 min, where the reaction time is deducted the time of adsorption equilibrium. However, there is almost no degradation as the solution with In_2S_3 nanoparticles which are obtained in pure ethanol. Moreover, after visible light irradiation 180 min, MO is just degraded by 40% over In_2S_3 sample collected in ethanol-water system (3:1), 66% for product in ethanol-water system (1:3) and 70% for the sample obtained in pure water. These results reveal that the as-synthesized 3D flowerlike In_2S_3 microspheres have the best photocatalytic activity for MO, which can be attributed to both the relative higher BET surface area and advantageous optical property. As to the photocatalytic mechanism of In_2S_3 on MO, Fu et al. verified that visible light excited In_2S_3 leads to formation of $\cdot\text{OH}$ radical and in turn oxidizes the organic compound pollutants by the generated $\cdot\text{OH}$ radical^[14, 56].



Finally, MO can be oxidized and mineralized to produce inorganic compounds, such as CO_2 , H_2O , NH_4^+ , SO_3^{2-} , and SO_4^{2-} . The possible overall reactions that occurred during this photocatalysis process could be proposed as shown in Equ. (4)-

(8):

Conclusions

In summary, 3D flowerlike $\beta\text{-In}_2\text{S}_3$ microspheres have been successfully synthesized by a facile thermal solution method only using ethanol-water as solvent. In this work, TAA not only acts as a sulfur source but also a ligand of In^{3+} , which plays an important part in the phase formation and the morphologies evolution of In_2S_3 . The reaction durations and solvent as well have a significant influence on the morphology of the In_2S_3 products. A morphology formation mechanism has been proposed and discussed on the basis of experimental data. Furthermore, the prepared 3D flowerlike In_2S_3 microspheres are applied in photocatalytic degradation of methyl orange and show relatively high visible-light photocatalytic activity, which can be attributed to both the large BET surface area and advantageous optical property. Our method is a simple and safe route that involves no complex or highly toxic reagents, surfactants or poisonous organic solvents. Therefore, it is very promising for simple, safe and low-cost industrial production.

Acknowledgments

This work was supported by the National Natural of Science Foundation of China (Grant No. 21371101), 111 Project (B12015) and MOE Innovation Team (IRT13022) of China.

Notes and references

- ^aDepartment of Materials Chemistry, Key Laboratory of Advanced Energy Materials Chemistry (MOE), TKL of Metal and Molecule-based Material Chemistry, College of Chemistry Nankai University, Tianjin, 300071, P. R. China.
- ^bCollaborative Innovation Center of Chemical Science and Engineering (Tianjin), Tianjin 300072, P. R. China.
- † Electronic Supplementary Information (ESI) available: [Figure S1: Fitting curve (26° to 29.5° in 2θ) of 3D flowerlike In_2S_3 . Figure S2: XRD patterns of samples synthesized at different reaction durations in ethanol-water system (1:1). Figure S3: Schematic diagram of a projected view as TAA adsorbed on the (222) surface of In_2S_3 to form a layer. Figure S4: XRD patterns of products obtained in ethanol-water system with the volume ratio of 1:0, 3:1, 1:3, 0:1. Figure S5: Time-dependent UV-vis absorption spectra using 3D flowerlike In_2S_3 as photocatalyst.]. See DOI: 10.1039/b000000x/
- 1 A. L. Linsebigler, G. Lu and J. T. Yates, *Chem. Rev.*, 1995, **95**, 735-758.
 - 2 W. Zhao, C. Chen, X. Li, J. Zhao, H. Hidaka and N. Serpone, *J. Phys. Chem. B*, 2002, **106**, 5022-5028.
 - 3 B. Öregan and M. Gratzel, *Nature*, 1991, **353**, 737-740.
 - 4 J. He, G. Benkö, F. Korodi, T. Polivka, R. Lomoth, B. Åkermarck, L. Sun, A. Hagfeldt and V. Sundström, *J. Am. Chem. Soc.*, 2002, **124**, 4922-4932.
 - 5 S. Rodrigues, K. T. Ranjit, S. Uma, I. N. Martyanov and K. J. Klabunde, *Adv. Mater.*, 2005, **17**, 2467-2471.
 - 6 R. Asahi, T. Morikawa, T. Ohwaki, K. Aoki and Y. Taga, *Science*, 2001, **293**, 269-271.
 - 7 S. U. M. Khan, M. Al-Shahry and W. B. Ingler, *Science*, 2002, **297**, 2243-2245.
 - 8 S. Sakthivel and H. Kisch, *Angew. Chem., Int. Ed.*, 2003, **42**, 4908-4911.
 - 9 Y. Bi, S. Ouyang, N. Umezawa, J. Cao and J. Ye, *J. Am. Chem. Soc.*, 2011, **133**, 6490-6492.
 - 10 D. Li, X. C. Duan, Q. Qin, H. M. Fan and W. J. Zheng, *Cryst. Eng. Comm.*, 2013, **44**, 8933-8936.

- 11 A. Kudo, K. Omori and H. Kato, *J. Am. Chem. Soc.*, 1999, **121**, 11459-11467.
- 12 Q. Li, B. D. Guo, J. G. Yu, J. R. Ran, B. H. Zhang, H. J. Yan and J. R. Gong, *J. Am. Chem. Soc.*, 2011, **133**, 10878-10884.
- 13 Z. X. Chen, D. Z. Li, W. J. Zhang, C. Chen, W. J. Li, M. Sun, Y. H. He and X. Z. Fu, *Inorg. Chem.*, 2008, **47**, 9766-9772.
- 14 Y. H. He, D. Z. Li, G. C. Xiao, W. Chen, Y. B. Chen, M. Sun, H. J. Huang, and X. Z. Fu, *J. Phys. Chem. C*, 2009, **113**, 5254-5262.
- 15 W. M. Du, J. Zhu, S. X. Li, and X. F. Qian, *Cryst. Growth. Des.*, 2008, **8**, 2130-2136.
- 16 S. Rengaraj, S. Venkataraj, C. W. Tai, Y. H. Kim, E. Repo, and M. Sillanpää, *Langmuir*, 2011, **27**, 5534-5541.
- 17 W. M. Qiu, M. S. Xu, X. Yang, F. Chen, Y. X. Nan, J. I. Zhang, H. Iwaic and H. Z. Chen, *J. Mater. Chem.*, 2011, **21**, 13327-13333.
- 18 Y. H. Kim, J. H. Lee, D.-W. Shin, S. M. Park, J. S. Moon, J. G. Nam and J.-B. Yoo, *Chem. Commun.*, 2010, **46**, 2292-2294.
- 19 G. Liu, X. Jiao, Z. Qin and D. Chen, *Cryst. Eng. Comm.*, 2011, **13**, 182-187.
- 20 F. M. Ye, C. Wang, G. H. Du, X. B. Chen, Y. J. Zhong and J. Z. Jiang, *J. Mater. Chem.*, 2011, **21**, 17063-17065.
- 21 L. Y. Chen, Z. D. Zhang and W. Z. Wang, *J. Phys. Chem. C*, 2008, **112**, 4117-4123.
- 22 B. Pejova and I. Bineva, *J. Phys. Chem. C*, 2013, **117**, 7303-7314.
- 23 J. Choi, J. Jin, J. Lee, J. H. Park, H. J. Kim, D. H. Oh, J. R. Ahn and S. U. Son, *J. Mater. Chem.*, 2012, **22**, 11107-11112.
- 24 G. Li and H. J. Liu, *J. Mater. Chem.*, 2011, **21**, 18398-18402.
- 25 L. N. Zhang, W. Zhang, H. B. Yang, W. Y. Fu, M. H. Li, H. Zhao and J. W. Ma, *Appl. Surf. Sci.*, 2012, **258**, 9018-9024.
- 26 A. W. Tang, F. Teng, Y. Wang, Y. B. Hou, W. Han, L. X. Yi and M. Y. Gao, *Nanoscale Res. Lett.*, 2008, **3**, 502-507.
- 27 S. Acharya, M. Dutta, S. Sarkar, D. Basak, S. Chakraborty, and N. Pradhan, *Chem. Mater.*, 2012, **24**, 1779-1785.
- 28 Y. J. Xiong, Y. Xie, G. A. Du and X. B. Tian, *J. Mater. Chem.*, 2002, **12**, 98-102.
- 29 M. F. Cansizoglu, R. Engelken, H. W. Seo and T. Karabacak, *ACS Nano.*, 2010, **4**, 733-740.
- 30 Y. H. Kim, J. H. Lee, D. W. Shin, S. M. Park, J. S. Moon, J. G. Nam and J. B. Yoo, *Chem. Commun.*, 2010, **46**, 2292-2294.
- 31 M. A. Franzman and R. L. Brutchey, *Chem. Mater.*, 2009, **21**, 1790-1792.
- 32 Y. N. Xia, P. D. Yang, Y. G. Sun, Y. Y. Wu, B. Mayers, B. Gates, Y. D. Yin, F. Kim and H. Q. Yan, *Adv. Mater.*, 2003, **15**, 353-389.
- 33 Z. L. Xiao, C. Y. Han, W. K. Kwok, H. H. Wang, U. Welp, J. Wang and G. W. Crabtree, *J. Am. Chem. Soc.*, 2004, **126**, 2316-2317.
- 34 D. X. Wu, J. F. Duan, C. Y. Zhang, K. Guo, and H. T. Zhu, *J. Phys. Chem. C*, 2013, **117**, 9121-9128.
- 35 J. Z. Jiang, J. Zou, Y. X. Zhang, J. N. Ma, H. P. Jiang and Q. J. Wan, *Mater. Lett.*, 2012, **79**, 132-135.
- 36 L. Liu, H. J. Liu, H. Z. Kou, Y. Q. Wang, Z. Zhou, M. M. Ren, M. Ge, and X. W. He, *Cryst. Growth. Des.*, 2009, **9**, 113-117.
- 37 P. Gao, Y. Xie, S. W. Chen and M. Z. Zhou, *Nanotechnology*, 2006, **17**, 320-324.
- 38 A. Datta, S. K. Panda, D. Ganguli, P. Mishra and S. Chaudhuri, *Cryst. Growth. Des.*, 2007, **7**, 163-169.
- 39 Y. Liu, H. Y. Xu and Y. T. Qian, *Cryst. Growth. Des.*, 2006, **6**, 1304-1307.
- 40 H. Zhu, X. L. Wang, W. Yang, F. Yang and X. R. Yang, *Mater. Res. Bull.*, 2009, **44**, 2033-2039.
- 41 S. Acharya, S. Sarkar and N. Pradhan, *J. Phys. Chem. Lett.*, 2012, **3**, 3812-3817.
- 42 Y. X. Sun, H. J. Zheng, X. C. Li, K. Zong, H. Wang, J. B. Liu, H. Yan and K. W. Li, *RSC Adv.*, 2013, **3**, 22095-22101.
- 43 X. L. Gou, F. Y. Cheng, Y. H. Shi, L. Zhang, S. J. Peng, J. Chen and P. W. Shen, *J. Am. Chem. Soc.*, 2006, **128**, 7222-7229.
- 44 J. Q. Yang, X. C. Duan, Q. Qin and W. J. Zheng, *J. Mater. Chem. A*, 2013, **1**, 7880-7884.
- 45 B. Zhang, X. C. Ye, W. Y. Hou, Y. Zhao and Y. Xie, *J. Phys. Chem. B*, 2006, **110**, 8978-8985.
- 46 X. M. Ni, Q. B. Zhao, H. G. Zheng, B. B. Li, J. M. Song, D. E. Zhang and X. J. Zhang, *Eur. J. Inorg. Chem.*, 2005, **23**, 4788-4793.
- 47 X. D. Liu, X. C. Duan, P. Peng and W. J. Zheng, *Nanoscale*, 2011, **3**, 5090-5095.
- 48 H. Zhang, D. Yang, X. Ma, Y. Ji, J. Xu and D. Que, *Nanotechnology*, 2004, **15**, 622-626.
- 49 J. M. Ma, Z. F. Liu, J. B. Lian, X. C. Duan, T. Kim, P. Peng, X. D. Liu, Q. Chen, G. Yao and W. J. Zheng, *Cryst. Eng. Comm.*, 2011, **13**, 3072-3079.
- 50 K. Egashira and N. Nishi, *J. Phys. Chem. B*, 1998, **102**, 4054-4057.
- 51 Y. X. Li, G. Chen, Q. Wang, X. Wang, A. K. Zhou and Z. Y. Shen, *Adv. Funct. Mater.*, 2010, **20**, 3390-3398.
- 52 N. Bao, L. Shen, T. Takata and K. Domen, *Chem. Mater.*, 2008, **20**, 110-117.
- 53 Q. Tian, M. Tang, Y. Sun, R. Zou, Z. Chen, M. Zhu, S. Yang, J. Wang, J. Wang and J. Hu, *Adv. Mater.*, 2011, **23**, 3542-3547.
- 54 W. T. Kim and C. D. Kim, *J. Appl. Phys.*, 1986, **60**, 2631-2633.
- 55 W. T. Bi, M. Zhou, Z. Y. Ma, H. Y. Zhang, J. B. Yu and Y. Xie, *Chem. Commun.*, 2012, **48**, 9162-9164.
- 56 X. Q. An, J. C. Yu, F. Wang, C. H. Li and Y. C. Li, *Appl. Catal. B: Environ.*, 2013, **129**, 80-88.

90